International Journal of Low-Carbon Technologies, 2025, **20**, 234–248
https://doi.org/10.1093/ijlct/ctae293
Original Article

Experimental validation of a simplified CFD model for a PCM-water finned heat exchanger

Francisco Javier González Gallero[1,*], Gabriel González Siles[1], Ismael Rodríguez Maestre[1], Juan Luis Foncubierta Blázquez[1], Michelle Bottarelli[2]

[1]Escuela Técnica Superior de Ingeniería de Algeciras, Universidad de Cádiz, Avenida Ramón Puyol, Algeciras 11202, Spain
[2]Department of Architecture, University of Ferrara, Via Quartieri 8, Ferrara 44121, Italy

*Corresponding author. Escuela Técnica Superior de Ingeniería de Algeciras, Universidad de Cádiz, Avenida Ramón Puyol, s/n. Algeciras 11202, Spain.
E-mail: javier.gallero@gm.uca.es

Abstract

The most widely used numerical models in the scientific literature for simulating heat exchangers with phase change materials (PCMs) and water as the heat transfer fluid, are based on computational fluid dynamics (CFD) techniques, with the modelling of phase change being the key issue. The consideration of phase change effect, as well as the resolution of the movement of the PCM in the liquid state, make CFD models computationally very expensive. However, various published experiments indicate that during the heat discharge process, the dominant heat transfer mechanism is conduction in the solidified PCM around the finned tube. For this reason, this article presents a simplified CFD model, where convective flow of the PCM is neglected during the discharge process. The model was validated experimentally, and to achieve this validation process, an experimental prototype of a one-meter-long axially finned heat exchanger with four fins was built. Inlet and outlet water temperatures were continuously recorded, along with temperatures at various points inside the PCM, under four different water flow rates. The proposed numerical model was able to predict the outlet water temperature with an error smaller than 1°C in all cases, and to capture the observed trend in temperature inside the PCM.

1 Introduction

Given the current energy context, regional, national, and international policies are increasingly focused on promoting energy production mainly from renewable sources [1]. Due to problems of matching supply and demand with renewable energies, efforts are being made to develop new energy storage systems, such as those based on phase change materials (PCMs) [2]. These materials store thermal energy by using the latent heat of phase transitions, achieving a higher energy density than the classical systems based on sensible heat storage [3].

However, due to their low thermal conductivity [4], the main challenge is to improve heat transfer, especially in those applications where thermal power requirements are higher, such as in the production of domestic hot water [5]. Thus, the development of this type of exchangers has intensified in recent years, and many related studies can be found in the scientific literature [6]. A wide variety of configurations and methods used for heat transfer intensification are shown in the review made by Al-Maghalseh *et al.* [7]: shell and tube exchangers in which the heat transfer fluid (HTF) is driven through a serpentine tube within the PCM [8]; filling the PCM with high thermal conductivity particles ([9, 10]) or integrating the PCM into metal foams [11]; PCM micro-encapsulation to maximize the heat transfer and the adaptation to volume variations [12], and those based on the use of fins to increase the contact surface area of the HTF pipe with the PCM [13].

Among finned heat exchangers, the axially finned exchanger is one of the most widely used [14]. Many studies on the influence of the axial fin geometry on the energy performance of the exchanger have been revised: corrugated design [15], Y-shaped design [16], single and double bifurcation fin configurations [17], etc. Yagci *et al.* [18] carried out heat transfer experiments with different tube surface configurations as finless tube and fin geometries with various edge lengths' ratios. The authors concluded there was no significant improvement in heat transfer with respect to straight fins with the same contact surface area. Therefore, this current work has been focused on a water–PCM exchanger with straight fins.

Regarding the thermal analysis of axially finned exchangers, it must consider both conductive and convective fluxes within three different domains (PCM, finned tubes and HTF) and two phases (solid and liquid), together with the PCM phase change process. This last process is a nonlinear shifting boundary problem that is governed by the rate at which the PCM is able to transfer latent heat. The problem is known as the Stefan problem [19] and, according to Rana *et al.* [20], the difficulty of modelling this process poses a challenge today. Because the analytical solutions are limited to simplified one-dimensional configurations [19], the analysis, design, and optimization of this kind of exchangers are approached through experiments or numerical simulations.

Received 26 July 2024; revised 18 November 2024; accepted 24 December 2024
© The Author(s) 2025. Published by Oxford University Press.
This is an Open Access article distributed under the terms of the Creative Commons Attribution Non-Commercial License (http://creativecommons.org/licenses/by-nc/4.0/), which permits non-commercial re-use, distribution, and reproduction in any medium, provided the original work is properly cited. For commercial re-use, please contact reprints@oup.com for reprints and translation rights for reprints. All other permissions can be obtained through our RightsLink service via the Permissions link on the article page on our site-for further information please contact journals.permissions@oup.com.

Downloaded from https://academic.oup.com/ijlct/article/doi/10.1093/ijlct/ctae293/7979319 by guest on 21 December 2025

Table 1. Description of the effective heat capacity method, the enthalpy method, and the heat source term method.

Effective heat capacity method	Enthalpy method	Heat source term method
Energy equation:	*Energy equation:*	*Energy equation:*
$\rho C_{eff}\frac{\partial T}{\partial t}=\vec{\nabla}\cdot\left(k\vec{\nabla}T\right)$	$\rho\frac{\partial h}{\partial t}=\vec{\nabla}\cdot\left(k\vec{\nabla}T\right)$	$\rho C_P\frac{\partial T}{\partial t}=\vec{\nabla}\cdot\left(k\vec{\nabla}T\right)-\rho L\frac{\partial f}{\partial t}$
Where:	*Where:*	*Where:*
$C_{eff}=\begin{cases} C_{p,s} & T<T_s \\ \frac{C_{p,s}+C_{p,l}}{2}+\frac{L}{T_l-T_s} & T_s\leq T<T_l \\ C_{p,l} & T\geq T_l \end{cases}$	$h=\begin{cases} \int_{T_0}^{T}C_{p,s}dT & T<T_s \\ \int_{T_0}^{T}C_{p,s}dT+L\frac{T-T_s}{T_l-T_s} & T_s\leq T<T_l \\ \int_{T_0}^{T_s}C_{p,s}dT+L+\int_{T_l}^{T}C_{p,l}dT & T\geq T_l \end{cases}$ $h\,(T_0)=0\;J\;kg^{-1}$	$f=\begin{cases} 0 & T<T_s \\ \frac{T-T_s}{T_l-T_s} & T_s\leq T<T_l \\ 1 & T\geq T_l \end{cases}$

With respect to experimental studies, they usually address both charge and discharge processes of different exchanger configurations and under different HTF flowrates and temperatures. Thus, Herbinger *et al.* [21] experimented with a finned-tube PCM-heat exchanger where the number of fins was varied from 4 to 8, to 12. The impact on exchanger performance of the geometry (number of finned tubes), system configuration (parallel or series), and operational parameters (initial temperature, HTF temperature, and HTF flowrate) was discussed. The authors concluded that the melting temperature differential (temperature difference between the HTF and the PCM) plays an important role in the characterization and power estimation of this kind of systems. Similarly, Pakalka *et al.* [22] experimentally compared two PCM-based copper heat exchangers with different geometrical parameters with the aim of finding the configuration with the fastest heat exchange and the lowest cost.

These experimental studies show that, although convection within the liquid PCM assists the phase transition [23], the addition of fins reduces the convective effects by partitioning the domain and constraining buoyancy-driven movements in the PCM [24]. This effect will be noticeable in the solidification processes, where convection tends to delay the onset of a well-defined solidification front. For this reason, the early appearance of a solidification front around the fins is favored in finned heat exchangers. The rapid generation of a solid PCM layer around the fins, combined with the low thermal conductivity characteristic of this kind of materials, makes conduction the dominant heat transfer mechanism in the PCM solidification process ([25, 26]).

On the other hand, numerical models are usually focused on the thermal analysis of the exchanger by using CFD techniques, where the key issue is the thermal and fluid dynamic modelling of the PCM phase change, which represents a moving-boundary problem. Three methods for the thermal modelling of the PCM, which allow a fixed-grid solution to be undertaken, are commonly applied [27]: the effective heat capacity method, the enthalpy method and the heat source term method (Table 1). The first one involves establishing an effective specific heat capacity (C_{eff}) for the material, typically consisting of a piecewise function that defines a specific heat for each phase: solid, liquid, and mushy zone, which separates the two phases. In the enthalpy method, the total enthalpy is obtained by integrating the specific heat capacity over the working interval and adding the latent heat in the mushy phase. This method accounts for the latent heat in the energy equation by assigning a nodal latent heat value to each computational cell according to the temperature of the cell. The governing equation is the same for both the solid and liquid phases, and the solid–liquid interface position is not explicitly tracked. A more detailed review of these two first methods can be found in Iten *et al.* [28]. The heat source term method is an alternative approach of enthalpy discretization where a temperature dependent liquid fraction function (f) controls the value of the source term included in the energy equation.

A significant challenge with grid-fixed solution methods lies in addressing the zero-velocity condition, a necessary requirement when the liquid region undergoes the transition to a solid state. Thus, different methods are used to switch off (or switch on) velocities in mesh cells that are freezing (or melting) [29]. Velocities can be set to zero when the mean latent heat content reaches some predetermined fraction of the latent heat of the phase change [30], or by driving the viscosity of the cell to a very large value as the latent heat content of the cell falls to zero [31]. Another approach involves modelling the cells undergoing a phase change as pseudo-porous media, with a porosity being a function of the nodal latent heat and ranging between 0 (fully solid) and 1 (fully liquid) [29]. Thus, the Darcy law's source term is added to the linear momentum equation to model the reduced porosity in the mushy zone [32]. From the reviewed scientific literature (Table 2), it can be concluded that the majority of numerical studies conducted for simulating the phase change transition of PCM in heat exchangers are based on this enthalpy-porosity method introduced by Brent *et al.* [29]. Unsteady Navier–Stokes (linear momentum) equations for nonisothermal incompressible fluids, with the Boussinesq approximation to model buoyancy effects, are frequently considered. Viscous dissipation is also commonly neglected in the energy equation. Some other key features of the reviewed numerical models have been presented in Table 2.

Trp *et al.* [33] used the enthalpy formulation to address the conjugate problem of transient forced convection and solid–liquid phase change heat transfer in a shell and tube latent thermal energy storage unit. The tubes had no fins, and authors formulated an axisymmetric 2D mathematical model of the shell and tube system to simulate charging and discharging processes in which convection in the liquid phase of the PCM was ignored. The errors made in the estimation of the outlet water temperature were not provided.

Downloaded from https://academic.oup.com/ijlct/article/doi/10.1093/ijlct/ctae293/7979319 by guest on 21 December 2025

Table 2. Description of CFD numerical studies on heat transfer in heat exchangers with PCM. NR stands for 'not reported'.

References, year		Trp *et al.* (2006, [33])	Tao *et al.* (2012, [34])	Hosseini *et al.* (2012 [35], 2014 [36])	Tao *et al.* (2015, [23])	Pahamli *et al.* (2016, [37])	Youssef *et al.* (2018, [38])	Li *et al.* (2019, [39])	Abidi *et al.* (2021, [40])	Monemi *et al.* (2023, [41])
System description		Shell and tube heat exchanger (energy storage unit)	Shell and (enhanced) tube heat exchanger (energy storage unit)	Horizontal shell and tube heat exchanger	Horizontal shell and (finned) tube heat exchanger	Horizontal shell and tube heat exchanger	PCM heat exchanger with spiral-wired tubes	Tube-fin cool storage heat exchanger	Horizontal shell and finned tube exchanger	Cross flow PCM-to-air and liquid finned heat exchanger
N° of fins / fin density		No fins	Modelled by changing heat transfer coefficient	No fins	3, 5, 7 (lower half) (axial fins)	No fins	24 (spiral) wire fins per turn	19 fins in 506 mm (radial fins)	12 (axial fins)	12 per inch (radial fins)
Heat transfer fluid (HTF)		Water	He/Xe mixture	Water	He/Xe mixture	Water	Water	Water	—	Air / Water
HTF flow rate		0.017 kg/s; 0.026 kg/s	NR	NR [35], 1 l/min [36]	NR	NR (Values of Re)	6–18 l/min	1.3 l/min, 2 l/min, 2.7 l/min	—	Air: 0.08 kg/s; 0.15 kg/s; 0.30 kg/s
PCM	**Material**	Mixture of fluoride salts (80.5% LiF and 19.5% CaF_2)	Paraffin Rubitherm RT 30	Paraffin wax, RT50 (Rubitherm GmbH)	Mixture of fluoride salts (80.5% LiF and 19.5% CaF_2)	RT50	PCM-A16	N° 28 paraffin	$CaCl_2.6H_2O$ (homogeneous mixture with Graphene nanoparticles)	Paraffin-based (Docosane)
	Density (kg m $^{-3}$) (liquid–solid)	2390	750–789	760–880	2390	780	800	774	1562–1802	820
	Specific heat capacity (J kg $^{-1}$ K^{-1}) (liquid–solid)	1770	2400–1800	2000	1770	2000	2370–2300	3200	2100–1400	2200
	Latent heat (kJ kg $^{-1}$)	816	206	160	816	168	213	200	192	234
	Melting temperature/ area (°C)	1667	27.6	45–51	1667	51	15–17	28	29	43.8
	Congealing temperature/ area (°C)	NR	NR	51–46	NR	45	17–15	28	29	43.8
	Conductivity (W m $^{-1}$ K^{-1}) (liquid–solid)	3.8	0.19–0.18	0.2	3.8	0.2	0.18	0.13–0.2	0.561–1.008	0.24–0.37
	Viscosity (Pa s)	0.00186	NR	0.0036–0.0052	0.00186	NR	NR	0.0055	0.0054	NR
Computational domain		PCM & Water	PCM & He/Xe mixture (1-D flow)	PCM	PCM & He/Xe mixture (1-D flow)	PCM & water (3-D flow)	PCM & water (3-D flow)	PCM & water	PCM	PCM & air/water
Process		Charge & discharge	Charge	Charge [35], charge & discharge [36]	Charge	Charge	Charge & discharge	Charge & discharge	Charge & discharge	Charge & discharge
Simulation domain/type	**2-D**	✓	✓		✓				✓	
	3-D			✓		✓	✓	✓		✓
	Unsteady	✓	✓	✓	✓	✓	✓	✓	✓	✓

(Continued)

Downloaded from https://academic.oup.com/ijlct/article/doi/10.1093/ijlct/ctae293/7979319 by guest on 21 December 2025

Table 2. Continued

References, year		Trp *et al.* (2006, [33])	Tao *et al.* (2012, [34])	Hosseini *et al.* (2012 [35], 2014 [36])	Tao *et al.* (2015, [23])	Pahamli *et al.* (2016, [37])	Youssef *et al.* (2018, [38])	Li *et al.* (2019, [39])	Abidi *et al.* (2021, [40])	Monemi *et al.* (2023, [41])
Linear momentum (liquid PCM)	Incompressible		✓	✓	✓	✓	✓	✓	✓	✓
	Newtonian		✓	✓	✓	✓	✓	✓	✓	✓
	Boussinesq approximation			✓	✓	✓	✓	✓	✓	✓
	Darcy's law source term			✓		✓	✓	✓	✓	✓
Energy	Enthalpy method	✓	✓	✓	✓	✓	✓	✓	✓	✓
	Viscous dissipation		NR	Neglected	Neglected	Neglected	Neglected	Neglected	Neglected	Neglected
Flow type		Laminar	NR	Laminar	Laminar	Laminar	Laminar (PCM) - Turbulent (water)	Laminar	Laminar	Laminar (PCM, water) - Turbulent (air)
Discretization method		Control Volume Approach	Finite Volume Method	Finite Volume Method	Finite Volume Method	Finite Volume Method	Finite Volume Method	Finite Volume Method	Finite Element Method	Finite Element Method
Software program		Self-written FORTRAN computer code	NR	In-house developed	NR	In-house developed	ANSYS Fluent	ANSYS Fluent	COMSOL Multiphysics 5.5	COMSOL Multiphysics 6.0
Solving algorithm		SIMPLER	NR	SIMPLE	NR	SIMPLE	PISO	Pressure-Based Method	NR	PARDISO
Mesh: Type; N° of mesh elements		Stagger grid; NR	300–4800	NR; ~300 000	Structured; ~96 000	Structured; 51 900	Unstructured; 920 703 – 1 981 116	NR	Unstructured; 120 000	Unstructured; ~6 000 000
Time step (s)		Dimensionless time step (0.06)	5	0.05	5	0.1	5	0.1	NR	NR
Convergence criterion (mass, momentum, energy)		10^{-6}	NR	10^{-7}	NR	10^{-5}, 10^{-5}, 10^{-7}	—, 10^{-3}, 10^{-4}	NR	NR	NR
Computational time		NR	NR	NR	NR	NR	NR	NR	2 h (CPUi7 and 16Gig DDR4 RAM)	NR
Validation methodology		Experiments [33] / PCM temperature variations.	Code validation.	Experiments [42] / Comparison of PCM average temperature profile.	Experiments [43] / Comparison of PCM temperature at reference points.	Experiments [35] / Comparison of PCM average temperature profile.	Experiments [38] / Comparison of PCM average temperature profile.	Experiments [44] / Comparison of melting front.	Experiments [45] / Qualitative comparison of melting front.	Experiments [46] / Comparison of air outlet temperature (relative errors smaller than 5%; absolute errors smaller than 1.5 °C)
Main conclusions		Operating conditions and geometric dimensions depend on the required heat transfer rate and time for energy storage or delivery.	Performance of the phase change thermal energy storage can be improved by using enhanced tubes while the increase in pressure drop may be neglected.	Solidification is dominated by conduction. Melting is initially dominated by conduction and soon after by convection.	Weak effects of liquid PCM natural convection on the total Latent Heat Storage rate. Fin parameters should be selected appropriately to ensure the uniformity of melting process.	Simultaneous increase in eccentricity and Stefan number lead to higher rate of melting process which is due to extended convection zone subjected to greater thermal potential.	The effects of the changes in HTF inlet flow rate and temperature in the sensible heat storage and release are not significant.	The PCM solidifies near the wall of the cooling water pipe and heat transfer is dominated by conduction in the solidification process.	Fin elongation speeds up phase change, reducing the charging and discharge process time.	Relationships between PCM phase change time, working fluid flow rate and outlet temperature.

Downloaded from https://academic.oup.com/ijlct/article/doi/10.1093/ijlct/ctae293/7979319 by guest on 21 December 2025

Hosseini *et al.* ([35, 36]) did a combined experimental and numerical study to analyze the melting and solidification of PCM inside a shell and tube heat exchanger. The authors observed that the inlet HTF temperature had a strong influence on the time required for the total phase change. They also concluded that PCM solidification was dominated by conduction, while convection was finally the prevailing heat transfer mechanism in the melting process. This behavior was also reported by Seddegh *et al.* [47] in their numerical analysis of heat transfer in a vertical cylindrical shell and unfinned tube latent heat energy storage unit. Furthermore, Pahamli *et al.* [37] in their study on a PCM-filled single-pass shell and tube heat exchanger, declared that conduction was even the dominated heat transfer mechanism at the end stages of the melting process. One of the interesting conclusions drawn by the study of Tao *et al.* [23] was that, since the effect of natural convection on the average heat storage was very limited, a two-dimensional axisymmetric model without considering the effects of natural convection can be a plausible approach in engineering applications for which the details of the solid–liquid interface are not relevant. In a previous work, Tao *et al.* [34] developed a simplified 2D model to simulate a shell and (enhanced) tube configuration in which the heat source term method was adopted to deal with the moving boundary problem in the solid–liquid phase change process. The effect of natural convection of PCM was neglected during melting, and heat transfer at the interface between the enhanced tubes and the PCM was modelled using existing correlations. The model was not validated experimentally but numerically.

On the other hand, Youssef *et al.* [38] developed a 3D CFD model of a spiral-wired tube in a PCM exchanger to enhance heat transfer within the PCM, and, although they found a noticeable influence of changes in inlet heat transfer fluid flow rate and temperature on the melting and solidification times, no significant effects were seen on the sensible heat storage and release. On the contrary, the work by Li *et al.* [39] found a subtle effect of the flow rate of the cooling water on the PCM solidification rate. A more significant effect was observed by increasing the mass fraction of graphene added to the PCM. Abidi *et al.* [40] also conducted a CFD study of an axially finned heat exchanger with a nano-PCM containing graphene nanoparticles. The Enthalpy Method was used to model heat conduction in the solid phase, where the dependence of the thermal capacity with temperature was adjusted using an expression analogous to a normal distribution. The thermal conductivity, the viscosity, and the density were calculated considering a mixture in which graphene nanoparticles were homogeneously distributed both in the solid and the liquid PCM. Specifically, the Maxwell model and the Brinkman model [48] were used to calculate the mixture conductivity and viscosity, respectively.

Abidi *et al.* [40] employed COMSOL Multiphysics 5.5 [49] and the finite element method for the 2D numerical simulations of a horizontal shell and finned tube exchanger. Their results were compared with the experimental observations provided by Chen *et al.* [45] of the melting/solidification fronts in the charge and discharge modes. According to the authors, the comparisons of the simulated fronts with photographs of the experiments at the same time showed acceptable similarities. A similar 3D CFD model was proposed by Momemi and Fartaj [41] to study a PCM-to-air and water-finned heat exchanger based on minichannels. The numerical results were validated using the experimental data provided by Fotowat *et al.* [46], with absolute and relative errors smaller than 1.5°C and 5%, respectively, in the prediction of heat transfer fluid outlet temperature.

In general, these numerical models have reported satisfactory results, but they are usually computationally expensive. Thus, even though, among the reviewed studies (Table 2), only the work by Abidi *et al.* [40] provided information about their 2D model solution time (about 2 h in a PC including a CPUi7 and 16Gb DDR4 RAM), much longer computation times (up to 27 h) have been found in other similar 3D models [50]. Also, based on the experimental knowledge and as pointed out by some authors (Tao *et al.* [23]), convective effects in the liquid PCM could be neglected to save computational cost in the modelling of finned tube exchangers, especially in the solidification process.

Thus, this article aims to present the development and implementation of a simplified CFD model of a longitudinally finned tube PCM-water heat exchanger, which will be used for general engineering applications such as DWH production. One of the main characteristics of the model proposed is that natural convection in the liquid phase of the PCM has been ignored. Although the justification for neglecting convection in the liquid PCM region has been highlighted and confirmed by former experimental and numerical studies, and this simplification has been employed in simpler numerical models, it has not been previously used in 3D CFD models of horizontal and longitudinally finned heat exchangers. Furthermore, the use of a piecewise-linear function that faithfully reproduces the actual dependence of the PCM's specific heat during the melting and solidification processes, provides the model with a higher degree of accuracy in estimating heat transfer. Another important objective has been the experimental validation of the proposed numerical model. Thus, an experimental prototype of the exchanger was created to test and corroborate this simplified approach under different water flow rates and charge and discharge processes. Given the small number of fins considered (4), it is expected that the restrictions of the fins to the liquid PCM natural convection and the reduction of the heat storage capacity are not weak and small.

First, a detailed presentation of the experimental study carried out to validate the proposed numerical model is given. Then, the computational model assumptions, domains, boundary conditions, and solving approaches are described. Finally, the experimental and numerical results are shown and discussed.

2 Experimental investigation and numerical modelling

This section begins by describing the experimental prototype of the water-PCM longitudinally finned tube heat exchanger built to experimentally validate the simplified CFD model. Then, the experimental setup and the set of experimental tests for model validation, divided into charge and discharge modes, are presented. Afterwards, the proposed numerical model (governing equations, assumptions, boundary conditions, etc.) used to simulate the system is shown.

2.1 Experimental prototype

The PCM-WATER heat exchanger prototype built for this study consists of a copper pipe with 4 axial fins, 1 m in length, an inner pipe diameter of 13 mm, an outer pipe diameter of

Downloaded from https://academic.oup.com/ijlct/article/doi/10.1093/ijlct/ctae293/7979319 by guest on 21 December 2025

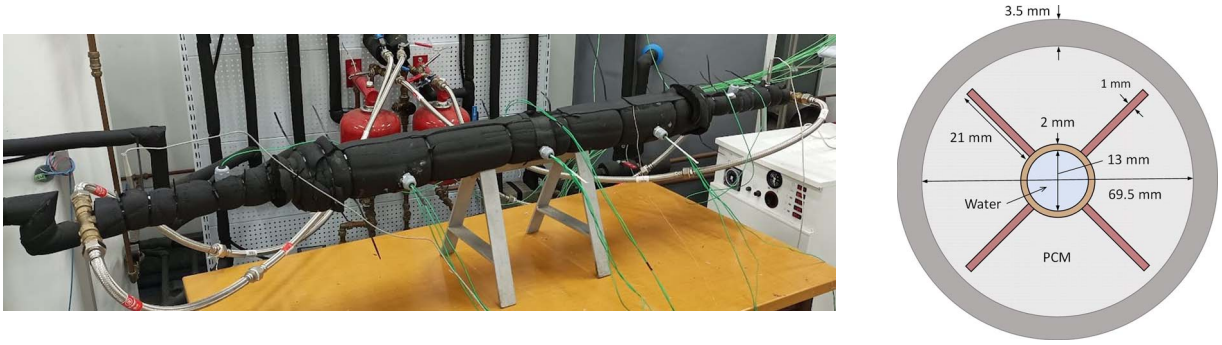

Figure 1. a) Photograph of the experimental prototype. b) Schematics of the exchanger cross-section (the external insulation layer is not shown).

Table 3. Rubitherm RT 54 HC thermal properties.

Property	54HC	Units
Melting area	53–54	°C
Congealing area	54–53	°C
Heat storage capacity*	200	kJ kg^{-1}
Density (solid)	850	kg m^{-3}
Density (liquid)	800	kg m^{-3}
Thermal conductivity	0.2	W m^{-1} K^{-1}
Specific heat capacity	2	kJ kg^{-1} K^{-1}

*Combination of latent and sensible heat in a temperature range of 46°C to 61°C.

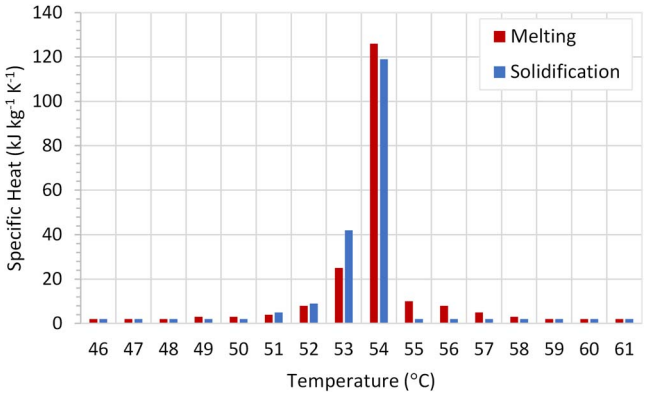

Figure 2. Rubitherm 54HC specific heat capacity as function of temperature (data from Rubitherm datasheet).

15 mm, a fin length of 21 mm, and a fin thickness of 1 mm. The fins are orientated at a 45° angle to the horizontal (Fig. 1). The outer pipe is made of steel with an inner diameter of 69.5 mm and a thickness of 3.5 mm. The external insulation layer, made of polyethylene (PE), has a thickness of 32 mm and a thermal conductivity of 0.038 W m^{-1} K^{-1}.

The Rubitherm RT 54 HC [4] has been used as the PCM material, and its main thermal characteristics are shown in Table 3. Figure 2 illustrates the specific heat capacity as a function of temperature for phase transitions (melting and solidification).

2.2 Experimental setup

The tests of the PCM-Water heat exchanger were conducted in an experimental facility (Fig. 3) developed by the Thermal Engineering Research Group at the University of Cádiz. The facility comprises two independent systems to produce hot and cold water. Each system includes a primary circuit for thermal energy production and a secondary circuit for connection to a prototype. Energy transfer between the primary and secondary circuits can occur instantly through a plate heat exchanger or via a 300-litre thermal storage tank.

Regarding the primary circuits, the production of cold water is carried out through an air-cooled chiller, Daikin EWQ016CAWP model, with a capacity of 16.8 kW and proportional control on the return water temperature. On the other hand, hot water production is achieved using an instantaneous electric boiler, the Elnur Gabarron model, with a capacity of 24 kW and on/off control with a 1°C hysteresis.

The secondary circuits providing cold and/or hot water to the prototype are equipped with a water circulation pump (Veneto AM-1 model with a maximum head and flow rate of 40 m and 40 l/min, respectively), controlled by variable-frequency drives (model ESPA Speedrive V2), flow meters (model Omega FP1402), and water temperature sensors.

For monitoring water flow rates and temperatures in both the primary and the secondary circuits, a data acquisition system OMB-DAQ-56 was employed, along with an expansion module OMB-PDQ1. This system includes a total of forty 22-bit analogue input channels with cold junction compensation for temperature measurements using thermocouples. The same data acquisition system is used to record measurements on the prototype itself.

For this study, 10 type K thermocouples have been installed: two of them at the water inlet (T_{in}) and the outlet (T_{out}) of the prototype, and the rest eight at three sections of the exchanger: one section at 16.6 cm (1/6 m) from the inlet, which was called here the inlet section (I); a second section at the middle (section M); and a third one (O) at 16.6 cm before the outlet. Temperature at these eight positions was named using three subscripts according to where the sensor was located: the first subscript indicates the section (I, M, or O); the second the direction (l for left and r for right); and the third whether the sensor was located in the first inner (1) or the second outer (2) ring (Fig. 4). These rings were equally spaced within the PCM domain.

Before conducting experimental tests on the heat exchanger, the TH-003 procedure [51], recommended by the Spanish National Metrology Centre, was used to calibrate the thermocouples. This procedure applies to all types of thermocouples, with or without compensation or extension cables, which are calibrated in isothermal environments of controlled temperature, baths, or furnaces, by comparison to calibrated standard thermometers referenced to the International Temperature

Downloaded from https://academic.oup.com/ijlct/article/doi/10.1093/ijlct/ctae293/7979319 by guest on 21 December 2025

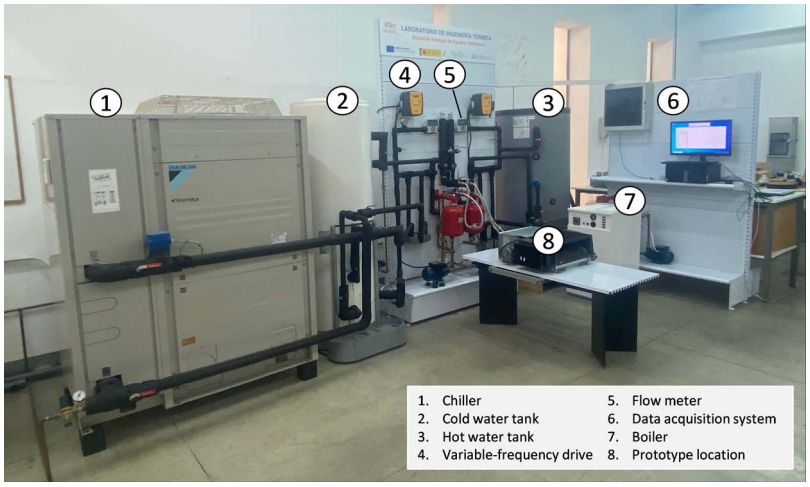

Figure 3. Experimental facility.

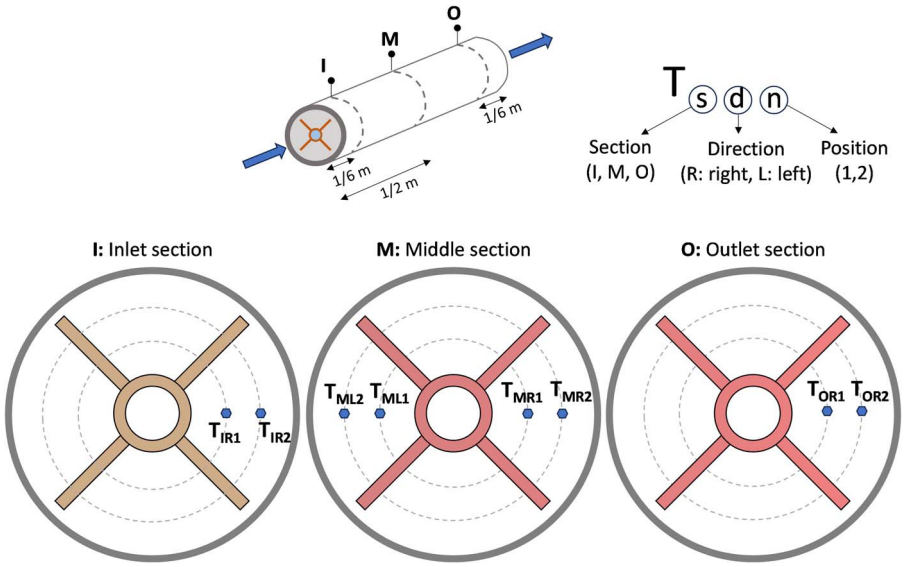

Figure 4. Location of temperature sensors and nomenclature. The external insulation layer is not shown.

Scale of 1990 (ITS-90). In this case, the average temperatures provided by two calibrated Negative Temperature Coefficient (NTC) thermistors, with an accuracy of ±0.2°C, were taken as the reference measurements. The following stages were followed:

- By using a water bath (model Nahita 602), a series of constant temperature equilibrium states were set, ranging from 0°C to 100°C at intervals of 5°C, approximately.
- For each equilibrium state, type K thermocouples connected to the data acquisition system were immersed, along with the NTC probes connected to a data logger with a valid calibration certificate and a total accuracy of ±0.38°C. The reading process was repeated for each calibration point. FIfteen calibration points were considered.
- The gain and offset of each thermocouple were obtained through a linear least-squares fit when compared with the reference measurements.
- A verification process was carried out at other 17 temperature values, covering the range of the experiment on the exchanger, and it was confirmed that the probes tested had a margin of error of 0.1°C compared to the calibrated standard.

Average discrepancies ranged from 0.2°C to 0.4°C. Specifically, for T_{in} and T_{out}, absolute differences ranged from 0.1°C to 0.5°C and from 0.0°C to 0.4°C, with average values of 0.16°C and 0.18°C, respectively.

2.2.1 Experimental tests

This section describes the experimental tests carried out with the prototype of the water-PCM heat exchanger to validate the proposed simplified numerical model. The system was subjected to competing cycles of charge and discharge. Four different water flow rates (3, 5, 10, and 15 l/min) were considered in the discharge mode. Reynolds number ranged from 4300 to 21 500.

The following stages were followed in all tests:

- Thermal equilibrium. In this stage, the whole system remains at rest until a uniform temperature is reached throughout the device.
- Charging mode. The following steps were taken at this stage: first, the desired flow rate is set in the secondary

Downloaded from https://academic.oup.com/ijlct/article/doi/10.1093/ijlct/ctae293/7979319 by guest on 21 December 2025

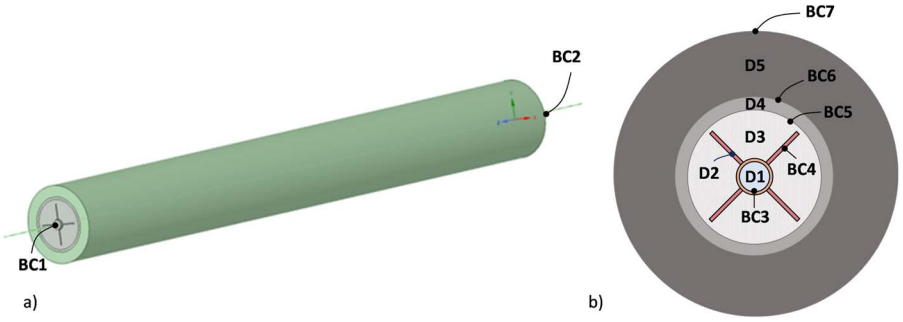

Figure 5. 3D computational domain of the water-PCM exchanger prototype.: a) Geometry. Inlet and outlet water boundary conditions are also shown. b) Cross-section. Domains and boundary conditions.

circuit by adjusting the variable-frequency drives and valves accordingly; then the heating process of the hot-water tank is initiated until the water temperature is 10°C above the PCM melting point. Then, the secondary circuit is activated, and the device charging begins. The experiment continues until reaching a PCM temperature 8°C above the melting point.

- Discharge mode. The discharge process starts by stopping the pumps of the secondary heat circuit. The desired flow rate is regulated in the secondary cold circuit, and cold water at around 16°C is passed through the prototype, except during the first few seconds due to the thermal inertia of the inlet pipe, exchanging heat with the cold tank prepared in the previous stage. Temperatures are recorded for 30 min.

Ambient temperature was also recorded. All records were made at 5-s intervals. To check the repeatability of the experiment, each of them was repeated at least three times. For the sake of clarity, a full record of one of the experiments is shown in the results section.

2.3 Simplified CFD model

The geometric and physical properties of the computational domain have attempted to replicate those of the experimental prototype of the water-PCM exchanger (Fig. 5). Details of the different subdomains and boundary conditions are given in Tables 4 and 5. ANSYS Fluent v17.1 was used for the CFD numerical simulations. This software uses the Green-Gauss finite volume method with a cell-centered formulation.

The present numerical study focused on simulating the discharge process, with the initial conditions for each domain established based on the experimental measurements at the end of the charging process.

Water flow has been resolved by discretizing the unsteady Navier–Stokes equations for incompressible fluid along with the k-ε turbulence model and standard wall functions. Conjugate heat transfer analysis has been used to include convective and conductive heat transfer at the fluid–solid interface. The inlet temperature and inlet flow rate were taken from the experiments. Outlet boundary condition was set as pressure outlet with a zero static gauge pressure.

Pressure–velocity coupling was solved by using the fluent pressure-based solver. Regarding the spatial discretization scheme, gradients were evaluated by the least squares cell-based method. A second-order scheme was used for pressure interpolation. Furthermore, second-order upwind scheme was applied to solve the linear momentum and energy equations. On the other hand, first-order upwind scheme was chosen for the discretization of the equations of turbulent kinetic energy and turbulent dissipation rate. Finally, a first-order implicit method was used for transient formulation.

The transient heat conduction equation has been solved both in the shell and finned tube and PCM, evaluating temperature gradients using the least-squares cell-based approach. Thermal and physical properties of the finned tube and shell correspond to copper and steel, respectively. Within the PCM, phase change is modelled by means of the Enthalpy Method. Thus, the temperature field is calculated from equation (1), which is solved using a fast implicit finite-difference method.

$$\rho \frac{\partial h}{\partial t} = \vec{\nabla} \cdot \left(k \vec{\nabla} T \right) \tag{1}$$

$$h(T) = \int_{T_0}^{T} C_{p,s}(T)\, dT \tag{2}$$

where $h(T_0)$ is zero at the reference temperature T_0 and $C_{p,s}(T)$ is the combination of latent and sensible heat extracted from the PCM manufacturer's data sheet and modelled as a piecewise-linear function (Fig. 2).

From a dynamic perspective, the PCM is treated as a solid, meaning that the velocity at all its points is zero.

On the outer surface of the insulation layer, a heat transfer coefficient was set according to Morgan's correlation for external natural convection [53], with the ambient air temperature equal to the recorded experimental value.

Initial conditions at the different parts of the computational domain were defined by the final state of the charge mode. Transient simulations were done with a time-step of 1 s and the convergence criteria were defined by setting the mass, momentum, and energy RSM target residuals to 10^{-4}, 10^{-4}, and 10^{-6}, respectively.

2.3.1 Grid independence study

Due to geometry complexity and considering computational cost, nonmatching unstructured meshes with predominantly hexahedral and tetrahedral elements within the finned pipe and PCM domains, respectively, were built (Fig. 6). The sweep method was used for the longitudinal direction. Grids were created ensuring a good spectrum of mesh quality metrics.

A mesh independence analysis was also conducted, focusing on the outlet water temperature (discharge process). The water flow rate was set to 3 l/min. Three meshes were generated with around 400 000, 800 000, and 4 800 000 elements, respectively. No significant differences in the outlet temperature were noticed using the medium and fine meshes as

Downloaded from https://academic.oup.com/ijlct/article/doi/10.1093/ijlct/ctae293/7979319 by guest on 21 December 2025

Table 4. Modelling description of the domains of the numerical model used for the simulation of the water-PCM exchanger.

Domain	Label	Modelling description	Equations [52]
Heat transfer fluid	D1	■ Water ■ Nonisothermal ■ Unsteady ■ Incompressible and Newtonian fluid ■ Turbulence model: k-ε	$\frac{\partial U_i}{\partial x_i} = 0; v_i = U_i + v_i'$ $\frac{\partial U_i}{\partial t} + U_j \frac{\partial U_i}{\partial x_j} = -\frac{1}{\rho_0}\frac{\partial P}{\partial x_i} + \frac{\partial}{\partial x_j}\left(\frac{\mu+\mu_t}{\rho_0}\frac{\partial U_i}{\partial x_j}\right)$ $\frac{\partial}{\partial t}(\rho e) + \frac{\partial}{\partial x_j}\left(U_j\ (\rho e + P)\right) = \frac{\partial}{\partial x_j}\left(k_{eff}\frac{\partial T}{\partial x_j}\right)$ $\frac{\partial K}{\partial t} + U_j\frac{\partial K}{\partial x_j} = \frac{2\mu_t}{\rho_0}\left(\frac{\partial U_i}{\partial x_j} + \frac{\partial U_j}{\partial x_j}\right)^2 - \varepsilon\frac{\partial}{\partial x_j}\left[\frac{1}{\rho_0}\left(\mu + \frac{\mu_t}{\sigma_K}\right)\frac{\partial K}{\partial x_j}\right]$ $\frac{\partial \varepsilon}{\partial t} + U_j\frac{\partial \varepsilon}{\partial x_j} = \frac{\varepsilon}{K}\left[C_{1\varepsilon}\frac{2\mu_t}{\rho_0}\left(\frac{\partial U_i}{\partial x_j} + \frac{\partial U_j}{\partial x_j}\right)^2 - C_{2\varepsilon}\right] - \frac{\partial}{\partial x_j}\left[\frac{1}{\rho_0}\left(\mu + \frac{\mu_t}{\sigma_\varepsilon}\right)\frac{\partial \varepsilon}{\partial x_j}\right]$ $k_{eff} = k + \frac{c_p\mu_t}{\mathrm{Pr}_t}, \mu_t = \rho C_\mu \frac{K^2}{\varepsilon}, \mathrm{Pr}_t = 0.85,$ $C_{1\varepsilon} = 1.44, C_{2\varepsilon} = 1.92, C_\mu = 0.09, \sigma_K = 1.0, \sigma_\varepsilon = 1.3,$
PCM	D3	■ RT 54 HC ■ Transient heat conduction ■ Phase transition: Enthalpy method ■ Solid and liquid phase at rest ($\mathbf{v} = 0$) ■ $C_{p,s}(T)$ piecewise-linear function of T (Fig. 2)	$\vec{v} = 0$ $\frac{\partial(\rho h)}{\partial t} = \vec{\nabla}\cdot\left(k\vec{\nabla}T\right)$ $h(T) = \int_{T_0}^{T} C_{p,s}(T)\ dT$
Finned tube	D2	■ Copper ■ Transient heat conduction	$\rho\frac{\partial h}{\partial t} = \vec{\nabla}\cdot\left(k\vec{\nabla}T\right)$ $h(T) = \int_{T_0}^{T} C_p\ dT$
Shell	D4	■ Steel ■ Transient heat conduction	
Insulation layer	D5	■ PVC ■ Transient heat conduction	

Table 5. Description of the boundary conditions of the numerical model used for the simulation of the water-PCM exchanger.

Boundary/interface	Label	Boundary/interface condition	Equations [52]
Water inlet	BC1	■ Fixed temperature (from experiments) ■ Fixed flow rate (from experiments)	$T_{BC1} = T_{exp}$ $\dot{m}_{BC1} = \dot{m}_{exp}$
Water outlet	BC2	■ Zero static gauge pressure	$P_{BC1} = P_0$
Water-tube	BC3	■ Conjugate heat transfer (convection and conduction)	$q_{BC3} = k_{eff}\left.\frac{\partial T}{\partial n}\right\|_{BC3}$
Finned tube-PCM	BC4		$T_t = T_{PCM}; q_t = q_{PCM}$
PCM-Shell	BC5	■ Thermal coupling (heat conduction)	$T_{PCM} = T_s; q_{PCM} = q_s$
Shell-insulation layer	BC6		$T_s = T_i; q_s = q_i$
Insulation layer-air	BC7	■ Free convection (Morgan's correlation [53])	$q_{BC3} = h_f\left(T_{BC7} - T_f\right)$

shown in Fig. 7. Therefore, the medium mesh was used for the remaining studies. The element size for this mesh varied between $1.2{\cdot}10^{-4}$ and $1.2{\cdot}10^{-2}$ m.

2.3.2 Validation of the PCM model

The thermal model used for the PCM will be tested by comparison with analytical and experimental solutions to certain heat transfer problems in the PCM.

Initially, the model's performance will be assessed by solving a transient 1D cooling problem of a semi-infinite PCM layer, for which an analytical solution exists [54]. This analytical solution was derived under certain assumptions [54]: negligible sensible heat stored compared to latent heat, absence of convection, the PCM initially being liquid and at its phase change temperature, and the temperature at the extreme of the semi-infinite layer being initially decreased and held constant thereafter. This approach, as outlined by Mehling and Cabeza [54], yielded a time-dependent function for the heat flux density through the PCM layer.

Subsequently, Fig. 8 presents a comparison between the analytical [54] and numerical solutions for the heat flux through the PCM layer over time. The root mean squared error (RMSE) value was found to be below 5 W/m^2. Absolute differences reached a plateau of around 5.5 W/m^2 early in the process, with a maximum value of 6.3 W/m^2 and relative errors smaller than 5%. Discrepancies between the two solutions can be attributed to the different approaches used to model the temperature-dependent specific heat capacity, where one is represented as a step function and the other as a Gaussian-type function (equation (1)).

Moreover, the accuracy of the numerical model's prediction of the solidification front was further assessed in a subsequent phase using experimental data provided by Ismail *et al.* [55]. The experiment focused on the discharge process of an AFHX

Downloaded from https://academic.oup.com/ijlct/article/doi/10.1093/ijlct/ctae293/7979319 by guest on 21 December 2025

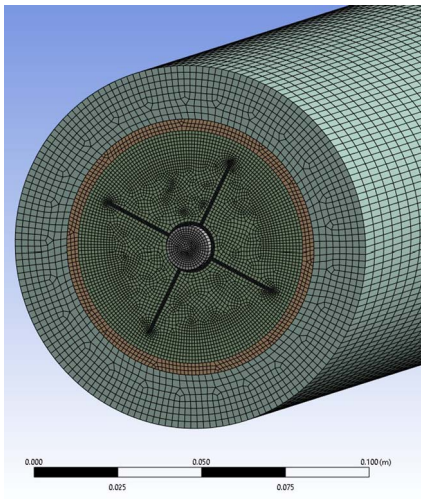

Figure 6. Final mesh of the system after the grid independence study.

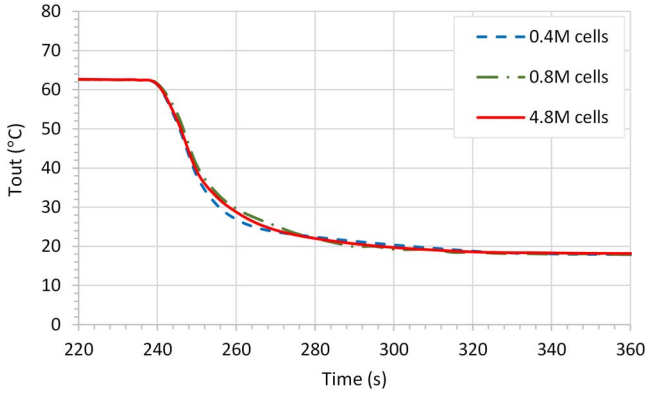

Figure 7. Grid sensitivity study.

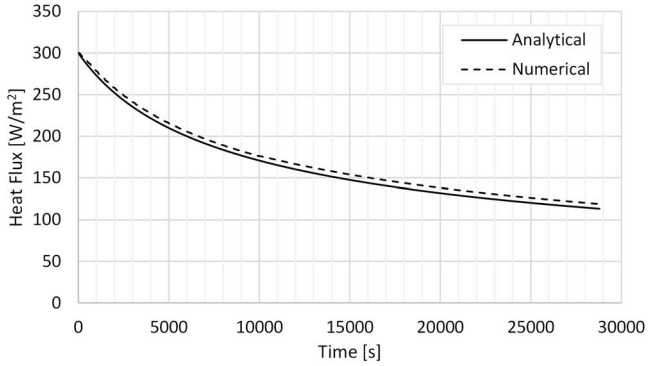

Figure 8. Heat flux as a function of time.

characterized by an inner diameter of 10 mm, an outer diameter of 37 mm, and four 10-mm long fins. The system operated with an initial temperature difference of 45.24°C between the PCM and the tube wall. The PCM employed was paraffin (code 130/135, Type 1) with a phase change temperature range of 55°C–57°C. The position of the solidification front over time served as an indicator of the model's accuracy.

Figure 9 illustrates the close resemblance between the numerical and experimental [55] results for the position of the solidification front at 30, 60, and 90 min. Consequently, the average relative error was only 2.8%. Therefore, it can be concluded that the PCM model is deemed satisfactory.

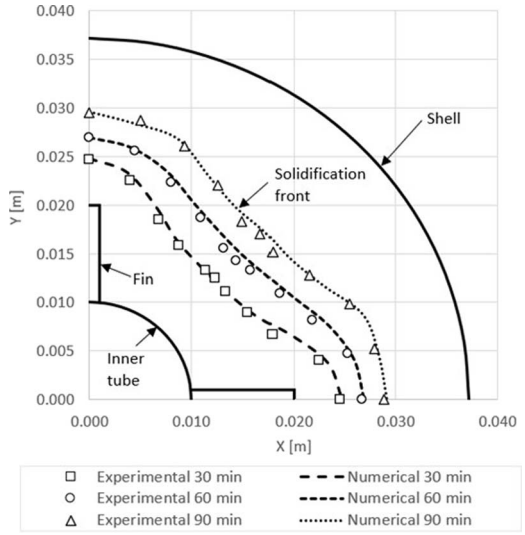

Figure 9. Numerical and experimental position of the solidification front with time.

3 Results and discussion

3.1 Experimental results

Figure 10 illustrates the experimental procedure described in the former section. Specifically, it shows the experimental results for a water flow of 3 l/min (discharge mode). The inlet and outlet water temperatures (T_{in} and T_{out}), the PCM temperatures at two points of the middle cross section (T_{MR1} and T_{MR2}) of the device, and the water flow rates during the charge (Q_c) and discharge (Q_d) processes are shown.

As observed, during the charging process, water was introduced at a flow rate of 15 l/min at a temperature of 63°C, approximately, which was well above the melting point of the PCM employed (54°C). In this case, the charging process was maintained for approximately 2.5 h to ensure the complete melting of the PCM. This melting process is reflected in the change of slope in the PCM temperature (T_{MR1} and T_{MR2}). The melting front reaches the position of thermocouple T_{MR1} around 15 min from the beginning of the experiment, when temperature changes are noticeable: a linear increase during the sensible heating, a flatter trend during the phase change until approximately minute 28, followed by a new increase due to sensible heating. The same pattern can be observed for T_{MR2}, with the melting process finishing 1 h later than in the case of T_{MR1}, since T_{MR2} is located farther away from the central pipe.

It is worth noting that since the modelling of the charging process was not the focus of this study, the charging flow rate was always set to the maximum to minimize the time for complete melting. Once the charge was completed, the flow of cold water (Q_d) began to circulate through the device. In this specific case, the flow rate was set at 3 l/min with an inlet temperature of approximately 15°C. Once again, the phase change can be seen at positions T_{MR1} and T_{MR2}. It can be observed that the outer point (T_{MR2}) does not reach complete solidification for the duration of the experiment.

Table 6 shows a brief descriptive analysis of the measured inlet and outlet water temperatures during the discharge process. Around 400 values were measured for each variable on average every 5 s. Maximum differences between the outlet and the inlet temperatures occurred at the beginning of the

Downloaded from https://academic.oup.com/ijlct/article/doi/10.1093/ijlct/ctae293/7979319 by guest on 21 December 2025

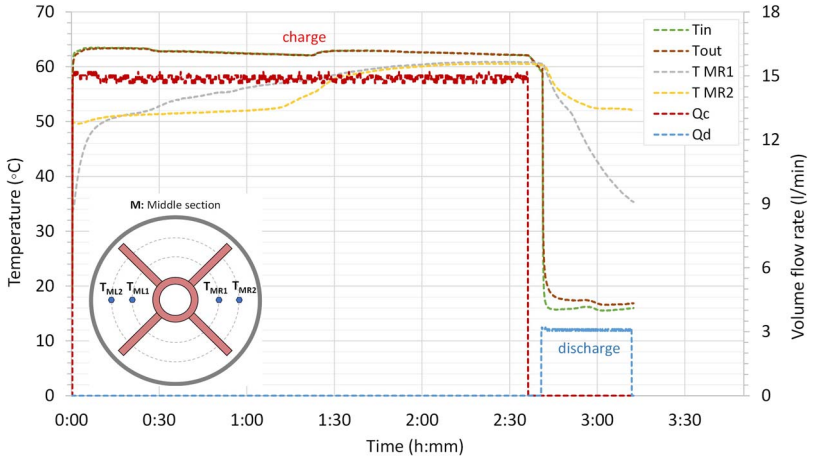

Figure 10. Example of the experimental observation for a full charge and discharge cycle. Cold water flow rate for the discharge process was set to 3 l/min.

Table 6. Statistical analysis of the experimental inlet and outlet water temperatures during the discharge processes.

Flow rate (l/min)	**3**			**5**			**10**			**15**		
Temperature (°C)	T_{in}	T_{out}	T_{out}-T_{in}	T_{in}	T_{out}	T_{out}-T_{in}	T_{in}	T_{out}	T_{out}-T_{in}	T_{in}	T_{out}	T_{out}-T_{in}
Minimum	15.5	16.5	0.8	15.9	16.9	0.6	16.2	16.8	0.1	16.7	17.2	0.0
Average	16.1	17.7	1.6	16.9	18.0	1.1	17.6	18.1	0.6	17.8	18.2	0.4
Maximum	54.6	59.6	10.4	56.3	61.5	10.3	62.3	62.4	2.6	58.6	58.9	1.1
SD	2.4	3.1	1.1	2.1	2.8	0.8	3.2	3.2	0.3	2.4	2.4	0.2
Median	15.8	17.4	1.2	16.5	17.3	0.8	17.3	17.8	0.4	17.7	18.1	0.3
IQR	0.3	0.8	0.7	0.9	1.0	0.5	1.1	1.1	0.2	0.9	0.8	0.2

SD stands for standard deviation and IQR is the interquartile range (the upper quartile minus the lower quartile).

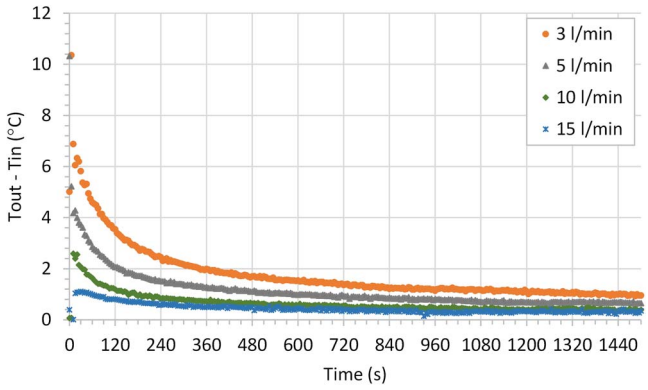

Figure 11. Time evolution of the measured outlet–inlet temperature difference.

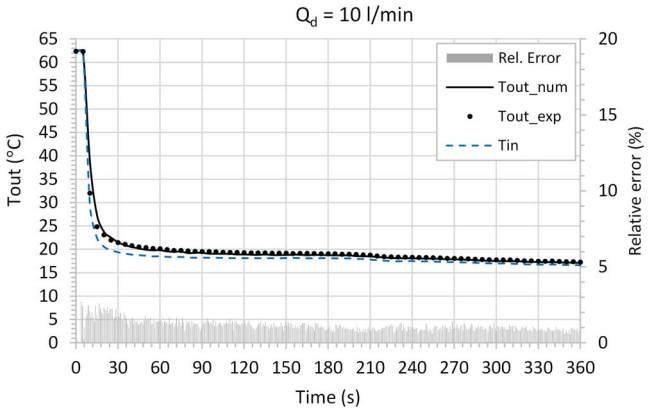

Figure 12. Experimental and numerical values of the outlet temperature for a water flow rate of 10 l/min.

process, and they were higher for smaller flow rates. They ranged from 1.1°C (for a flow rate of 15 l/min) to 10.4°C (3 l/min).

The time evolution of the difference between the measured outlet and inlet water temperature, which is directly related to the heat power transferred to the water flow, is shown in Fig. 11 for all water flow rates. At the beginning, temperature gradients between the PCM and the water are higher but as the device discharges, the inlet and outlet temperatures tend to approach each other, reducing the difference between them.

3.2 CFD simulation results

Figure 12 shows the experimental values of the outlet (T_{out_exp}) water temperature together with the simulation results of the outlet temperature (T_{out_num}) for the discharge process with a (cold) water flow rate (Q_d) of 10 l/min. There is a high correlation between the experimental and numerical values, with a root mean square error (RMSE) of 0.4°C, which is within the range of the experimental uncertainty of the thermocouples (0.4°C). Relative errors are smaller than 3%. A similar behavior has been observed for the remaining discharge flow rates.

Table 7 provides the values of the absolute and relative errors and RMSEs for the numerical outlet temperature when compared with the experimental results for the different water flow rates tested. Error values are generally very small, and they decrease as the flow rate increases.

Downloaded from https://academic.oup.com/ijlct/article/doi/10.1093/ijlct/ctae293/7979319 by guest on 21 December 2025

Table 7. Maximum absolute and relative errors and RMSEs for the simulated outlet water temperature. $\Delta T_{out} = |T_{out\_num} - T_{out\_exp}|$.

Q_d (l/min)	$(\Delta T_{out})_{max}$ (°C)	$(\Delta T_{out}/T_{out\_exp})_{max}$ (%)	RSME (°C)
3	1.0	4.1	0.4
5	0.8	4.1	0.3
10	0.5	2.6	0.2
15	0.2	3.7	0.2

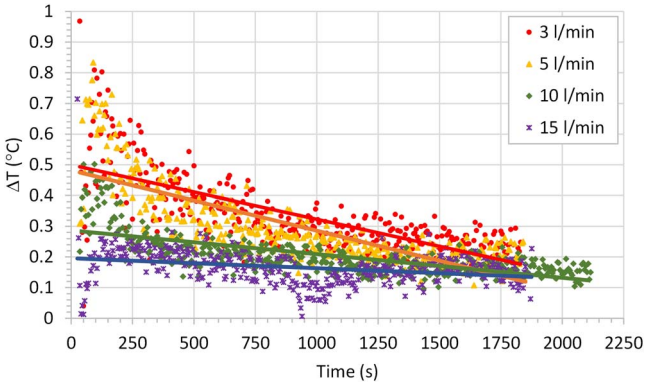

Figure 13. Absolute error of outlet–inlet temperature difference as a function of time.

The error made in estimating the water temperature differences between the inlet and the outlet is equal to ΔT_{out} ($|T_{out\_num} - T_{out\_exp}|$), since the numerical and experimental values of the inlet temperature are the same. Thus, Fig. 13 shows the time dependence of the absolute error of this temperature difference. As also shown in Table 7, the maximum absolute error does not exceed 1°C in any of the experiments.

The corresponding relative errors are smaller than 4.2%. Additionally, the linear trend (solid) lines of the absolute errors for each flow rate have also been plotted in Fig. 13. It can be observed that the error decreases over time for all the studied cases. This effect is also noticeable in the flow rate variation. A downward trend in the error is also observable as the discharge flow rate increases. The increase in flow rate improves thermal transfer, and thus, ΔT decreases more rapidly.

Figure 14 depicts PCM temperature at the different points tested for a cold-water flow rate of 5 l/min. It is observed that, considering the strong simplifications adopted for modelling the PCM thermal behavior, the model can predict temperature trends within the PCM satisfactorily. The same holds true for the rest of the experiments (with flow rates 3, 10 and 15 l/min).

3.3 Model use and limitations

According to the previous results, the model would be suitable for analyzing the discharge process of configurations in PCM-integrated heat exchangers where the design and properties of the PCM limit the fluid movement, reducing heat transfer by convection. Common cases would include:

- Heat exchangers with PCM confined in narrow or thin spaces. In configurations such as thin-layer PCM panels or small tubes.

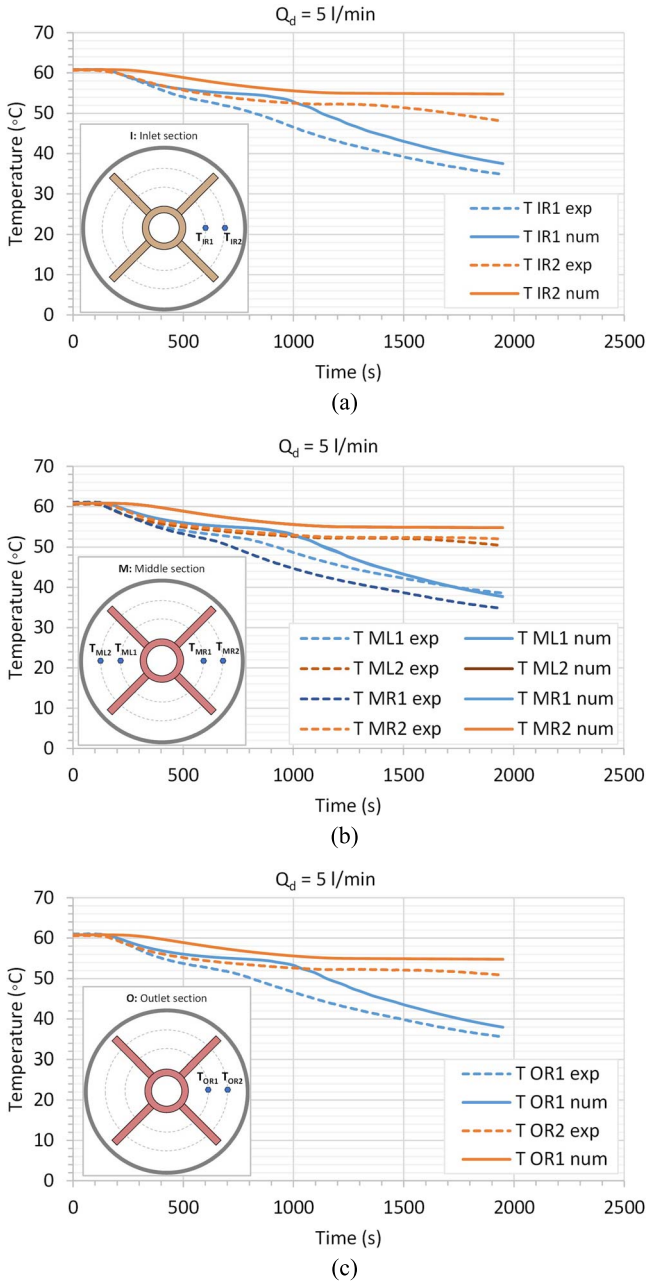

Figure 14. Temperature at: a) Inlet section; b) Middle section; c) Outlet section. Water flow rate of 5 l/min.

- PCM with high viscosity in liquid phase, such as certain phase-change oils or waxes with dense molecular structures.
- Heat exchangers in horizontal orientation or with limited natural convection.
- Porous structures or materials with high thermal conductivity in the PCM. Materials such as expanded graphite or metallic foams distribute heat by conduction without requiring convection.

On the other hand, the model would not be applicable to heat exchangers with large PCM volumes or significant thickness, where temperature gradients within the fluid could induce natural convective currents. It would also be ineffective for vertically oriented exchangers that enhance natural convection, or for PCMs with low viscosity in the liquid phase.

Downloaded from https://academic.oup.com/ijlct/article/doi/10.1093/ijlct/ctae293/7979319 by guest on 21 December 2025

4 Conclusions

In this study, a simplified CFD-based model of a water-PCM finned tube exchanger is presented and validated experimentally. The primary and simplifying assumption adopted in this model is that, during the discharge process, the convective effects of the PCM confined between the fins are negligible compared to the conduction mechanism in the PCM solid layer formed around the fins.

For the experimental validation, a longitudinally finned cylindrical heat exchanger of 1 m in length, featuring an inner copper pipe with four fins and an outer steel shell with respective inner diameters of 13 and 69.5 mm, was manufactured. The PCM used was Rubitherm RT 54 HC. Different tests with full cycles of charge and discharge of this prototype were conducted in an experimental facility of the Thermal Engineering Research Group at the University of Cádiz. The melting (charging) and solidification (discharge) processes of the PCM were monitored by recording the inlet and outlet water temperatures and the temperatures at eight points inside the PCM in three cross-sections of the tube, and at two different depths. Four different discharge flow rates (3, 5, 10, and 15 l/min) were considered.

The simplified numerical model was able to predict the water outlet temperature during discharge with a maximum error of 1°C, and an average RMSE in all experiments of 0.3°C. Relative errors were smaller than 4.2%, therefore smaller than those made by more complex models where convective flows within the PCM were considered. Furthermore, and despite the limitations of the simplified model, it can predict the temperature trends inside the PCM even when convective movement in the liquid phase is neglected. In this regard, the authors believe that these results could be improved for heat exchangers having a greater number of fins, where the fluid would even be more confined. The horizontal position of the exchanger, which minimizes buoyancy effects, could be another reason for the good performance of the numerical model. Thus, various experimental tests with different numbers of fins, along with the extension of the study to other PCM materials and other orientations of the heat exchanger to analyze the influence of gravity, are currently being investigated.

Author contributions

Francisco Javier González Gallero (Formal Analysis [equal], Investigation [equal], Methodology [equal], Supervision [equal], Writing—original draft [equal], Writing—review & editing [equal]), Gabriel González Siles (Data curation [equal], Validation [equal]), Ismael Rodríguez Maestre (Conceptualization [equal], Formal Analysis [equal], Investigation [equal], Methodology [equal]), Juan Luis Foncubierta Blázquez (Formal Analysis [equal], Investigation [equal], Writing—original draft [equal]), and Michelle Bottarelli (Formal Analysis [supporting], Writing—review & editing [supporting]).

Conflict of interest

None declared.

Funding

Grant Ref. PID2021-123562OB-I00 funded by MCIN/AEI/10.13039/501100011033 and by the European Union.

References

1. I. Energy Agency, Net zero by 2050 - a roadmap for the global energy sector. 2050. www.iea.org/reports/net-zeroby-2050
2. Baljit SSS, Chan HY, Sopian K. Review of building integrated applications of photovoltaic and solar thermal systems. *J Clean Prod* 2016;**137**:677–89. https://doi.org/10.1016/j.jclepro.2016.07.150.
3. Liu L, Hammami N, Trovalet L. *et al.* Description of phase change materials (PCMs) used in buildings under various climates: a review. *J Energy Storage* 2022;**56**:107560. https://doi.org/10.1016/j.est.2022.105760.
4. Rubitherm GmbH. https://www.rubitherm.eu/.
5. Zahir MH, Irshad K, Shafiullah M. *et al.* Challenges of the application of PCMs to achieve zero energy buildings under hot weather conditions: a review. *J Energy Storage* 2023;**64**:107156. https://doi.org/10.1016/j.est.2023.107156.
6. Ibrahim NI, Al-Sulaiman FA, Rahman S. *et al.* Heat transfer enhancement of phase change materials for thermal energy storage applications: a critical review. *Renew Sustain Energy Rev* 2017;**74**:26–50. https://doi.org/10.1016/j.rser.2017.01.169.
7. Al-Maghalseh M, Mahkamov K. Methods of heat transfer intensification in PCM thermal storage systems: review paper. *Renew Sustain Energy Rev* 2018;**92**:62–94. https://doi.org/10.1016/j.rser.2018.04.064.
8. Mahdi MS, Mahood HB, Alammar AA. *et al.* Numerical investigation of PCM melting using different tube configurations in a shell and tube latent heat thermal storage unit. *Therm Sci Eng Prog* 2021;**25**:101030. https://doi.org/10.1016/j.tsep.2021.101030.
9. Sandeep Kumar M, Murali Krishna V. Experimental investigation on performance of hybrid PCM's on addition of Nano particles in thermal energy storage. 2019. www.sciencedirect.comwww.materialstoday.com/proceedings
10. Chibani A, Mecheri G, Dehane A. *et al.* Industrial-scale for hydrogen charging in activated carbon (AX-21)-phase change material-nano-oxides systems. *J Energy Storage* 2023;**65**:107326. https://doi.org/10.1016/j.est.2023.107326.
11. Sheikh Y, Fatih Orhan M, Kanoglu M. Heat transfer enhancement of a bio-based PCM/metal foam composite heat sink. *Therm Sci Eng Prog* 2022;**36**:101536. https://doi.org/10.1016/j.tsep.2022.101536.
12. Soares N, Rosa N, Costa JJ. *et al.* Validation of different numerical models with benchmark experiments for modelling microencapsulated-PCM-based applications for buildings. *Int J Therm Sci* 2021;**159**:106565. https://doi.org/10.1016/j.ijthermalsci.2020.106565.
13. Abhinand S, Sharma A, Hardik B. *et al.* Performance analysis of PCM melting in a fin-assisted thermal energy storage system – a numerical study. *Int Commun Heat Mass Transf* 2023;**144**:106747. https://doi.org/10.1016/j.icheatmasstransfer.2023.106747.
14. Tao YB, He YL. A review of phase change material and performance enhancement method for latent heat storage system. *Renew Sustain Energy Rev* 2018;**93**:245–59. https://doi.org/10.1016/j.rser.2018.05.028.
15. Aly KA, El-Lathy AR, Fouad MA. Enhancement of solidification rate of latent heat thermal energy storage using corrugated fins. *J Energy Storage* 2019;**24**:100785. https://doi.org/10.1016/j.est.2019.100785.
16. Lohrasbi S, Sheikholeslami M, Ganji DD. Discharging process expedition of NEPCM in fin-assisted latent heat thermal energy storage system. *J Mol Liq* 2016;**221**:833–41. https://doi.org/10.1016/j.molliq.2016.06.044.
17. Sciacovelli A, Gagliardi F, Verda V. Maximization of performance of a PCM latent heat storage system with innovative fins. *Appl Energy* 2015;**137**:707–15. https://doi.org/10.1016/j.apenergy.2014.07.015.
18. Yagci OK, Avci M, Aydin O. Melting and solidification of PCM in a tube-in-shell unit: effect of fin edge lengths' ratio. *J Energy Storage* 2019;**24**:100802. https://doi.org/10.1016/j.est.2019.100802.

Downloaded from https://academic.oup.com/ijlct/article/doi/10.1093/ijlct/ctae293/7979319 by guest on 21 December 2025

19. Carslaw HS, Jaeger JC. *Conduction of Heat in Solids*. Oxford: Oxford University Press, 1959.
20. Rana S, Zunaid M, Kumar R. CFD analysis for heat transfer comparison in circular, rectangular and elliptical tube heat exchangers filled with PCM. *Mater Today Proc* 2022;**56**:637–44. https://doi.org/10.1016/j.matpr.2021.12.412.
21. Herbinger F, Groulx D. Experimental comparative analysis of finned-tube PCM-heat exchangers' performance. *Appl Therm Eng* 2022;**211**:118532. https://doi.org/10.1016/j.applthermaleng.2022.118532.
22. Pakalka S, Valančius K, Streckienė G. Experimental comparison of the operation of PCM-based copper heat exchangers with different configurations. *Appl Therm Eng* 2020;**172**:115138. https://doi.org/10.1016/j.applthermaleng.2020.115138.
23. Tao YB, He YL. Effects of natural convection on latent heat storage performance of salt in a horizontal concentric tube. *Appl Energy* 2015;**143**:38–46. https://doi.org/10.1016/j.apenergy.2015.01.008.
24. Solomon GR, Velraj R. Analysis of the heat transfer mechanisms during energy storage in a phase change material filled vertical finned cylindrical unit for free cooling application. *Energ Conver Manage* 2013;**75**:466–73. https://doi.org/10.1016/j.enconman.2013.06.044.
25. K Ismail, C Alves, and M Modesto. Numerical and experimental study on the solidication of PCM around a vertical axially finned isothermal cylinder. 2001. www.elsevier.com/locate/apthermeng
26. Dhaidan NS, Khodadadi JM. Improved performance of latent heat energy storage systems utilizing high thermal conductivity fins: a review. *J Renew Sustain Energy* 2017;**9**:034103. https://doi.org/10.1063/1.4989738.
27. Reji Kumar R, Samykano M, Pandey AK. *et al.* Phase change materials and nano-enhanced phase change materials for thermal energy storage in photovoltaic thermal systems: a futuristic approach and its technical challenges. *Renew Sustain Energy Rev* 2020;**133**:110341. https://doi.org/10.1016/j.rser.2020.110341.
28. Iten M, Liu S. A work procedure of utilising PCMs as thermal storage systems based on air-TES systems. *Energ Conver Manage* 2014;**77**:608–27. https://doi.org/10.1016/j.enconman.2013.10.012.
29. Brent AD, Voller VR, Reid KJ. Enthalpy-porosity technique for modeling convection-diffusion phase change: application to the melting of a pure metal. *Numerical Heat Transfer* 1988;**13**:297–318. https://doi.org/10.1080/10407788808913615.
30. Morgan K. A numerical analysis of freezing and melting with convection. *Comput Methods Appl Mech Eng* 1981;**28**:275–84. https://doi.org/10.1016/0045-7825(81)90002-5.
31. D. K. Gartling. "Finite element analysis of convective heat transfer problems with change of phase," in *Conference on numerical methods in laminar and turbulent flow*, Swansea, UK, 1978, p. 365, **12**, 382, https://doi.org/10.1016/0045-7825(77)90024-X.
32. Amagour MEH, Rachek A, Bennajah M. *et al.* Experimental investigation and comparative performance analysis of a compact finned-tube heat exchanger uniformly filled with a phase change material for thermal energy storage. *Energ Conver Manage* 2018;**165**:137–51. https://doi.org/10.1016/j.enconman.2018.03.041.
33. Trp A, Lenic K, Frankovic B. Analysis of the influence of operating conditions and geometric parameters on heat transfer in water-paraffin shell-and-tube latent thermal energy storage unit. *Appl Therm Eng* 2006;**26**:1830–9. https://doi.org/10.1016/j.applthermaleng.2006.02.004.
34. Tao YB, He YL, Qu ZG. Numerical study on performance of molten salt phase change thermal energy storage system with enhanced tubes. *Sol Energy* 2012;**86**:1155–63. https://doi.org/10.1016/j.solener.2012.01.004.
35. Hosseini MJ, Ranjbar AA, Sedighi K. *et al.* A combined experimental and computational study on the melting behavior of a medium temperature phase change storage material inside shell and tube heat exchanger. *Int Commun Heat Mass Transf* 2012;**39**:1416–24. https://doi.org/10.1016/j.icheatmasstransfer.2012.07.028.
36. Hosseini MJ, Rahimi M, Bahrampoury R. Experimental and computational evolution of a shell and tube heat exchanger as a PCM thermal storage system. *Int Commun Heat Mass Transf* 2014;**50**:128–36. https://doi.org/10.1016/j.icheatmasstransfer.2013.11.008.
37. Pahamli Y, Hosseini MJ, Ranjbar AA. *et al.* Analysis of the effect of eccentricity and operational parameters in PCM-filled single-pass shell and tube heat exchangers. *Renew Energy* 2016;**97**:344–57. https://doi.org/10.1016/j.renene.2016.05.090.
38. Youssef W, Ge YT, Tassou SA. CFD modelling development and experimental validation of a phase change material (PCM) heat exchanger with spiral-wired tubes. *Energ Conver Manage* 2018;**157**:498–510. https://doi.org/10.1016/j.enconman.2017.12.036.
39. Li D, Yang C, Yang H. Experimental and numerical study of a tube-fin cool storage heat exchanger. *Appl Therm Eng* 2019;**149**:712–22. https://doi.org/10.1016/j.applthermaleng.2018.12.024.
40. Abidi A, Rawa M, Khetib Y. *et al.* Simulation of melting and solidification of graphene nanoparticles-PCM inside a dual tube heat exchanger with extended surface. *J Energy Storage* 2021;**44**:103265. https://doi.org/10.1016/j.est.2021.103265.
41. Momeni M, Fartaj A. Numerical thermal performance analysis of a PCM-to-air and liquid heat exchanger implementing latent heat thermal energy storage. *J Energy Storage* 2023;**58**:106363. https://doi.org/10.1016/j.est.2022.106363.
42. Agyenim F, Eames P, Smyth M. Experimental study on the melting and solidification behaviour of a medium temperature phase change storage material (erythritol) system augmented with fins to power a LiBr/H2O absorption cooling system. *Renew Energy* 2011;**36**:108–17. https://doi.org/10.1016/j.renene.2010.06.005.
43. Lacroix M. Numerical simulation of a shell-and-tube latent heat thermal energy storage unit. *Sol Energy* 1993;**50**:357–67. https://doi.org/10.1016/0038-092X(93)90029-N.
44. Arasu AV, Mujumdar AS. Numerical study on melting of paraffin wax with Al 2O 3 in a square enclosure. *Int Commun Heat Mass Transf* 2012;**39**:8–16. https://doi.org/10.1016/j.icheatmasstransfer.2011.09.013.
45. Chen G, Sun G, Jiang D. *et al.* Experimental and numerical investigation of the latent heat thermal storage unit with PCM packing at the inner side of a tube. *Int J Heat Mass Transf* 2020;**152**:119480. https://doi.org/10.1016/j.ijheatmasstransfer.2020.119480.
46. Fotowat S, Askar S, Fartaj A. Experimental transient response of a minichannel heat exchanger with step flow variation. *Exp Therm Fluid Sci* 2017;**89**:128–39. https://doi.org/10.1016/j.expthermflusci.2017.08.004.
47. Seddegh S, Wang X, Henderson AD. Numerical investigation of heat transfer mechanism in a vertical shell and tube latent heat energy storage system. *Appl Therm Eng* 2015;**87**:698–706. https://doi.org/10.1016/j.applthermaleng.2015.05.067.
48. Lauriat G, Prasad V. Non-Darcian effects on natural convection in a vertical porous enclosure. *Int J Heat Mass Transf* 1989;**32**:2135–48. https://doi.org/10.1016/0017-9310(89)90120-8.
49. www.comsol.com. COMSOL AB, COMSOL Multiphysics®. Stockholm, Sweden.
50. Herbinger F, Bhouri M, Groulx D. Investigation of heat transfer inside a PCM-air heat exchanger: a numerical parametric study. *Heat and Mass Transfer* 2018;**54**:2433–42. https://doi.org/10.1007/s00231-017-2101-9.
51. Centro Español de Metrología. TH-003 Procedimiento Para la calibración por comparación de termopares. 2011.
52. ANSYS FLUENT 12.0/12.1 Documentation. https://www.afs.enea.it/project/neptunius/docs/fluent/.
53. Morgan VT. The overall convective heat transfer from smooth circular cylinders. *Adv Heat Transf* 1975;**11**:199–264. https://doi.org/10.1016/S0065-2717(08)70075-3.

Downloaded from https://academic.oup.com/ijlct/article/doi/10.1093/ijlct/ctae293/7979319 by guest on 21 December 2025

54. Mehling H, Cabeza LF. *Heat and cold storage with PCM: an up to date introduction into basics and applications*. Springer, 2008.
55. Ismail KAR, Alves CLF, Modesto MS. Numerical and experimental study on the solidification of PCM around a vertical axially finned isothermal cylinder. *Appl Therm Eng* 2001;**21**:53–77. https://doi.org/10.1016/S1359-4311(00)00002-8.

Downloaded from https://academic.oup.com/ijlct/article/doi/10.1093/ijlct/ctae293/7979319 by guest on 21 December 2025

© The Author(s) 2025. Published by Oxford University Press. This is an Open Access article distributed under the terms of the Creative Commons Attribution Non-Commercial License (http://creativecommons.org/licenses/by-nc/4.0/), which permits non-commercial re-use, distribution, and reproduction in any medium, provided the original work is properly cited. For commercial re-use, please contact reprints@oup.com for reprints and translation rights for reprints. All other permissions can be obtained through our RightsLink service via the Permissions link on the article page on our site-for further information please contact journals.permissions@oup.com.
International Journal of Low-Carbon Technologies, 2025, 20, 234–248
https://doi.org/10.1093/ijlct/ctae293
Original Article